

# 1 Neutralising antibodies drive Spike mediated SARS-CoV-2 evasion

2

3 Kemp SA<sup>1\*</sup>, Collier DA<sup>1,2,3\*</sup>, Datir R<sup>1,2,3</sup>, Gayed S<sup>4</sup>, Jahun A<sup>5</sup>, Hosmillo M<sup>5</sup>, Ferreira IATM<sup>2,3</sup>,  
4 Rees-Spear C<sup>1</sup>, Mlcochova P<sup>2,3</sup>, Ines Ushiro Lumb<sup>6</sup>, David Roberts<sup>6</sup>, Anita Chandra<sup>2,3</sup>,  
5 Temperton N<sup>7</sup>, The CITIID-NIHR BioResource COVID-19 Collaboration<sup>8</sup>, The COVID-19  
6 Genomics UK (COG-UK) Consortium<sup>9</sup>, Sharrocks K<sup>4</sup>, Blane E<sup>3</sup>, Briggs JAG<sup>10</sup>, van Gils MJ<sup>11</sup>,  
7 Smith KGC<sup>2,3</sup>, Bradley JR<sup>3,12</sup>, Smith C<sup>14</sup>, Goldstein RA<sup>1</sup>, Goodfellow IG<sup>5</sup>, Smielewska A<sup>5,13</sup>,  
8 Skittrall JP<sup>4,14,15</sup>, Gouliouris T<sup>4</sup>, Gkrania-Klotsas E<sup>4</sup>, Illingworth CJR<sup>14,16</sup>, McCoy LE<sup>1</sup>, Gupta  
9 RK<sup>2,3,16,17</sup>

10

11 <sup>1</sup>Division of Infection and Immunity, University College London, London, UK.

12 <sup>2</sup> Cambridge Institute of Therapeutic Immunology & Infectious Disease (CITIID), Cambridge,  
13 UK.

14 <sup>3</sup>Department of Medicine, University of Cambridge, Cambridge, UK.

15 <sup>4</sup>Department of Infectious Diseases, Cambridge University NHS Hospitals Foundation Trust,  
16 Cambridge, UK.

17 <sup>5</sup>Department of Pathology, University of Cambridge, Cambridge

18 <sup>6</sup>Public Health England, Colindale, London, UK

19 <sup>7</sup>Viral Pseudotype Unit, Medway School of Pharmacy, University of Kent, UK

20 <sup>8</sup>The CITIID-NIHR BioResource COVID-19 Collaboration, see appendix 1 for author list

21 <sup>9</sup>The COVID-19 Genomics UK (COG-UK) Consortium, Full list of consortium names and  
22 affiliations are in the appendix

23

24 <sup>10</sup>Medical Research Council Laboratory of Molecular Biology, Cambridge, UK.

25 <sup>11</sup>Department of Medical Microbiology, Academic Medical Center, University of Amsterdam,  
26 Amsterdam Institute for Infection and Immunity, Amsterdam, Netherlands

27 <sup>12</sup> NIHR Cambridge Clinical Research Facility, Cambridge, UK.

28 <sup>13</sup>Department of Virology, Cambridge University NHS Hospitals Foundation Trust

29 <sup>14</sup>Department of Applied Mathematics and Theoretical Physics, University of Cambridge, UK

30 <sup>15</sup>Clinical Microbiology and Public Health Laboratory, Addenbrookes' Hospital, Cambridge, UK

31 <sup>16</sup> MRC Biostatistics Unit, University of Cambridge, Cambridge, UK

32 <sup>17</sup>Africa Health Research Institute, Durban, South Africa

33 **NOTE:** This preprint reports new research that has not been certified by peer review and should not be used to guide clinical practice.  
**\*equal contribution**

34

35 **Address for correspondence:**

36 Ravindra K. Gupta

37 Cambridge Institute for Therapeutic Immunology and Infectious Diseases

38 Jeffrey Cheah Biomedical Centre

39 Puddicombe Way

40 Cambridge CB2 0AW, UK

41 Tel: +44 1223 331491

42 [rkg20@cam.ac.uk](mailto:rkg20@cam.ac.uk)

43

44 **Key words: SARS-CoV-2; COVID-19; antibody escape, Convalescent plasma; neutralising**  
45 **antibodies; mutation; evasion; resistance; immune suppression**

46

47 **Abstract**

48 SARS-CoV-2 Spike protein is critical for virus infection via engagement of ACE2, and amino  
49 acid variation in Spike is increasingly appreciated. Given both vaccines and therapeutics are  
50 designed around Wuhan-1 Spike, this raises the theoretical possibility of virus escape,  
51 particularly in immunocompromised individuals where prolonged viral replication occurs.  
52 Here we report fatal SARS-CoV-2 escape from neutralising antibodies in an immune  
53 suppressed individual treated with convalescent plasma, generating whole genome ultradeep  
54 sequences by both short and long read technologies over 23 time points spanning 101 days.  
55 Little evolutionary change was observed in the viral population over the first 65 days despite  
56 two courses of remdesivir. However, following convalescent plasma we observed dynamic  
57 virus population shifts, with the emergence of a dominant viral strain bearing D796H in S2  
58 and  $\Delta$ H69/ $\Delta$ V70 in the S1 NTD of the Spike protein. As serum neutralisation waned, viruses  
59 with the escape genotype diminished in frequency, before returning during a final,  
60 unsuccessful course of convalescent plasma. *In vitro*, the Spike escape variant conferred  
61 decreased sensitivity to multiple units of convalescent plasma/sera from different recovered  
62 patients, whilst maintaining infectivity similar to wild type. These data reveal strong positive  
63 selection on SARS-CoV-2 during convalescent plasma therapy and identify the combination of  
64 Spike mutations D796H and  $\Delta$ H69/ $\Delta$ V70 as a broad antibody resistance mechanism against  
65 commonly occurring antibody responses to SARS-CoV-2.

## 66 Introduction

67 SARS-CoV-2 is an RNA betacoronavirus, with closely related viruses identified in pangolins and  
68 bats <sup>1,2</sup>. RNA viruses have inherently higher rates of mutation than DNA viruses such as  
69 Herpesviridae <sup>3</sup>. The capacity for successful adaptation is exemplified by the Spike D614G  
70 mutation, that arose in China and rapidly spread worldwide <sup>4</sup>, now accounting for more than  
71 90% of infections. The mutation appears to increase infectivity and transmissibility in animal  
72 models <sup>5</sup>. Although the SARS-CoV-2 Spike protein is critical for virus infection via engagement  
73 of ACE2, substantial Spike amino acid variation is being observed in circulating viruses <sup>6</sup>.  
74 Logically, mutations in the receptor binding domain (RBD) of Spike are of particular concern  
75 due to the RBD being targeted by neutralising antibodies and therapeutic monoclonal  
76 antibodies.

77

78 Deletions in the N-terminal domain (NTD) of Spike S1 are also being increasingly recognised,  
79 both within hosts <sup>7</sup> and across individuals <sup>8</sup>. The evolutionary basis for the emergence of  
80 deletions is unclear at present, and could be related to escape from immunity or to enhanced  
81 fitness/transmission. The most notable deletion in terms of frequency is  $\Delta$ H69/ $\Delta$ V70. This  
82 double deletion has been detected in multiple unrelated lineages, including the recent  
83 'Cluster 5' mink related strain in the North Jutland region of Denmark  
84 ([https://files.ssi.dk/Mink-cluster-5-short-report\\_AFO2](https://files.ssi.dk/Mink-cluster-5-short-report_AFO2)). There it was associated with the RBD  
85 mutation Y453F in almost 200 individuals. Another European cluster in GISAID includes  
86  $\Delta$ H69/ $\Delta$ V70 along with the RBD mutation N439K.

87

88 Although  $\Delta$ H69/ $\Delta$ V70 has been detected multiple times, within-host emergence remains  
89 undocumented and the reasons for its selection are unknown. Here we document real time  
90 SARS-CoV-2 emergence of  $\Delta$ H69/ $\Delta$ V70 in response to convalescent plasma therapy in an  
91 immunocompromised human host treated with the B cell depletion agent rituximab,  
92 demonstrating broad antibody escape in combination with the S2 mutation D796H.

93

## 94 Results

### 95 Clinical case history of SARS-CoV-2 infection in setting of immune-compromised host

96 These details are available on request from the authors.

97

98 **Negative SARS-CoV-2 specific antibodies and requirement for convalescent plasma (CP)**

99 We measured blood parameters including serum SARS-CoV-2 specific antibodies over time  
100 (Supplementary table 1, Supplementary Figure 1, 2). Imaging was consistent with COVID-19  
101 disease (Supplementary Figure 3). Total serum antibodies to SARS-CoV-2 were tested at days  
102 44 and 50 by S protein immunoassay (Siemens). Results were negative. Three units (200mL  
103 each) of convalescent plasma (CP) from three independent donors were obtained from the  
104 NHS Blood and Transfusion Service and administered on compassionate use basis. These had  
105 been assayed for antibody titres using the validated Euroimmun assay (Supplementary figure  
106 3). Patient serum was subsequently positive for SARS-CoV-2 specific antibodies by S protein  
107 immunoassay (Siemens) in the hospital diagnostic laboratory on days 68, 90 and 101.

108

109 **Virus genomic comparative analysis of 23 sequential respiratory samples over 101 days**

110 The majority of samples were respiratory samples from nose and throat or endotracheal  
111 aspirates during the period of intubation. Ct values ranged from 16-34 and all 23 respiratory  
112 samples were successfully sequenced by standard long read approach as per the ARTIC  
113 protocol implemented by COG-UK; of these 20 additionally underwent short-read deep  
114 sequencing using the Illumina platform. There was generally good agreement between the  
115 methods, though as expected nanopore demonstrated greater error at low variant  
116 frequencies (<10%) (Supplementary Figure 4). We detected no evidence of recombination,  
117 based on two independent methods.

118

119 Maximum likelihood analysis of patient-derived whole genome consensus sequences  
120 demonstrated clustering with other local sequences from the same region (Figure 1A). The  
121 infecting strain was assigned to lineage 20B bearing the D614G Spike variant. Environmental  
122 sampling showed evidence of virus on surfaces such as telephone and call bell but not in air  
123 on days 59, 92 and 101. Sequencing of these surface viruses showed clustering with those  
124 derived from the respiratory tract (Figure 1B). All samples were consistent with having arisen  
125 from a single viral population. In our phylogenetic analysis, we included sequential sequences  
126 from three other local patients identified with persistent viral RNA shedding over a period of  
127 4 weeks or more (Supplementary Table 2). Viruses from these individuals showed very little  
128 divergence in comparison to the case patient (Figure 1B) and none showed amino acid  
129 changes in Spike over time. We additionally inferred a maximum likelihood phylogeny

130 comparing sequences from these three local individuals and two long term  
131 immunosuppressed SARS-CoV-2 ‘shedders’ recently reported<sup>7,9</sup>, (Figure 1B). While the  
132 sequences from Avanzato et al showed a pattern of evolution more similar to two of the three  
133 other local patients, the case patient showed significant diversification with a mutation rate  
134 of 30 per year (Supplementary table 2).

135  
136 Further investigation of the sequence data suggested the existence of an underlying structure  
137 to the viral population in our patient, with samples collected at days 93 and 95 being rooted  
138 within, but significantly divergent from the original population (Figure 1B and 2A). The  
139 relationship of the divergent samples to those at earlier time points rules out the possibility  
140 of superinfection. The increased divergence of sequences does not necessarily indicate  
141 selection; a spatially compartmentalised subset of viruses, smaller in number than the main  
142 viral population, would be expected to evolve more quickly than the main population due to  
143 the increased effect of genetic drift<sup>10,11</sup>.

#### 144 145 **Virus population structure changes following convalescent plasma and remdesivir**

146 All samples tested positive by RT-PCR and there was no sustained change in Ct values  
147 throughout the 101 days following the first two courses of remdesivir (days 41 and 54), or the  
148 first two units of convalescent plasma (days 63 and 65). According to nanopore data, no  
149 polymorphisms occurred over the first 60 days at consensus level (Figure 2A). However, short  
150 read deep sequence Illumina data revealed minority polymorphisms in the viral population  
151 during this period (Figure 2B). For example, T39I in ORF7a reached a majority frequency of  
152 77% on day 44, arising *de novo* and increased in frequency during the first period of the  
153 infection (Supplementary Figure 6).

154  
155 In contrast to the early period of infection, between days 66 and 82 a dramatic shift in virus  
156 population structure was observed, with the near-fixation of D796H in S2 along with  
157  $\Delta$ H69/ $\Delta$ V70 in the S1 N-terminal domain (NTD) at day 82. This was identified in a nose and  
158 throat swab sample with high viral load as indicated by Ct of 23 (Figure 3). The deletion was  
159 not detected at any point prior to the day 82 sample, even as minority variants by short read  
160 deep sequencing.

161

162 On Days 86 and 89, viruses collected were characterised by the Spike mutations Y200H and  
163 T240I, with the deletion/mutation pair observed on day 82 having fallen to very low  
164 frequency. Sequences collected on these days formed a distinct branch at the bottom of the  
165 phylogeny in Figure 3, but were clearly associated with the remainder of the samples,  
166 suggesting that they did not result from superinfection (Supplementary Figure 7), and further  
167 were not significantly divergent from the bulk of the viral population (Supplementary Figure  
168 5).

169  
170 Sequencing of a nose and throat swab sample at day 93 again showed D796H along with  
171  $\Delta$ H69/ $\Delta$ V70 at <10% abundance, along with an increase in a virus population characterised  
172 by Spike mutations P330S at the edge of the RBD and W64G in S1 NTD. This new lineage  
173 reached near 100% abundance at day 93. Viruses with the P330S variant were detected in  
174 two independent samples from different sampling sites, ruling out the possibility of  
175 contamination. The divergence of these samples from the remainder of the population  
176 (Figure 3B), noted above, suggests the possibility of their resulting from the stochastic  
177 emergence, in the upper respiratory tract, of a previously unobserved subpopulation of  
178 viruses (Supplementary Figure 5).

179  
180 Following the third course of remdesivir (day 93) and third CP (day 95), we observed a re-  
181 emergence of the D796H +  $\Delta$ H69/ $\Delta$ V70 viral population. The inferred linkage of D796H and  
182  $\Delta$ H69/ $\Delta$ V70 was maintained as evidenced by the highly similar frequencies of the two  
183 variants, suggesting that the third unit of CP led to the re-emergence of this viral strain under  
184 renewed positive selection. Ct values remained low throughout this period with  
185 hyperinflammation, eventually leading to multi-organ failure and death at day 102. The  
186 repeated increase in frequency of the novel viral strain during CP therapy strongly supports  
187 the hypothesis that the deletion/mutation combination conferred antibody escape  
188 properties.

189  
190  **$\Delta$ H69/ $\Delta$ V70 + D796H confers impaired neutralisation by multiple convalescent plasma units**  
191 **and sera from recovered COVID-19 patients**

192 Using lentiviral pseudotyping we expressed wild type and  $\Delta$ H69/ $\Delta$ V70 + D796H mutant Spike  
193 protein in enveloped virions and compared neutralisation activity of CP against these viruses.

194 This system has been shown to give similar results to replication competent virus<sup>12,13</sup>. We first  
195 tested infection capacity over a single round of infection and found that  $\Delta$ H69/ $\Delta$ V70 + D796H  
196 had similar infectivity to wild type (both in a D614G background, Figure 4A, B). The  
197  $\Delta$ H69/ $\Delta$ V70 + D796H mutant was partially resistant to the first two CP units (Figure 4C, Table  
198 1A). In addition, patient derived serum from days 64 and 66 (one day either side of CP2  
199 infusion) similarly showed lower potency against the mutant (Figure 4C, Table 1A). The  
200 repeated observation of D796H +  $\Delta$ H69/ $\Delta$ V70 emergence and positive selection strengthens  
201 the hypothesis that these variants were the key drivers of antibody escape. Experimentally,  
202 the D796H +  $\Delta$ H69/ $\Delta$ V70 mutant also demonstrated reduced susceptibility to the CP3  
203 administered on day 95, explaining its re-emergence (Figure 4C, Table 1A).

204

205 Given reduced susceptibility of the mutants to at least two units of CP, and the expansion of  
206 sequences bearing  $\Delta$ H69/ $\Delta$ V70, we hypothesised that this represented a broad escape  
207 mechanism. We therefore screened antiviral neutralisation activity in sera from five  
208 recovered patients against the mutant and wild type viruses (Figure 4D). We observed that  
209 the mutant was indeed significantly less susceptible to four of five randomly selected sera,  
210 with the fifth showing reduced susceptibility that did not reach statistical significance (Table  
211 1B). Fold change reductions in susceptibility of the mutant were as high as ten-fold compared  
212 to wild type (Table 1B).

213

214 In order to probe the impact of the D796H and  $\Delta$ H69/ $\Delta$ V70 mutations on potency of  
215 monoclonal antibodies (mAbs) targeting Spike, we screened neutralisation activity of a panel  
216 of seven neutralizing mAbs across a range of epitope clusters<sup>13</sup> (Figure 4E). We observed no  
217 differences in neutralisation between single mutants and wild type, suggesting that the  
218 mechanism of escape was likely outside these epitopes.

219

220 In order to understand the mechanisms that might confer resistance to antibodies we  
221 examined a published Spike structure and annotated it our residues of interest (Figure 5).  
222 This analysis showed that  $\Delta$ H69/ $\Delta$ V70 is in a disordered, glycosylated loop at the very tip of  
223 the NTD, and therefore could alter binding of antibodies.  $\Delta$ H69/V70 is close to the binding  
224 site of the polyclonal antibodies derived from COV57 plasma, indicating the sera tested here  
225 may contain similar antibodies<sup>14,15</sup>. D796H is in an exposed loop in S2 (Figure 5), and appears



226 to be in a region frequently targeted by antibodies<sup>16</sup>, despite mutations at position 796 being  
227 rare (Supplementary table 4).

228

## 229 **Discussion**

230 Here we have documented a repeated evolutionary response by SARS-CoV-2 against antibody  
231 therapy during the course of a persistent and eventually fatal infection in an  
232 immunocompromised host. The observation of potential selection for specific variants  
233 coinciding with the presence of antibodies from convalescent plasma is supported by the  
234 experimental finding of reduced susceptibility of these viruses to plasma. Further, we were  
235 able to document real-time emergence of a variant  $\Delta$ H69/ $\Delta$ V70 in the NTD of Spike that has  
236 been increasing in frequency in Europe. In the case we report that it was not clear that the  
237 emergence of the antibody escape variant was the primary reason for treatment failure.  
238 However, given that both vaccines and therapeutics are aimed at Spike, our study raises the  
239 possibility of virus evasion, particularly in immune suppressed individuals where prolonged  
240 viral replication occurs.

241

242 Our observations represent a very rare insight, and only possible due to lack of antibody  
243 responses in the individual following administration of the B cell depleting agent rituximab  
244 for lymphoma, and an intensive sampling course undertaken due to concerns about  
245 persistent shedding and risk of nosocomial transmission. Persistent viral replication and the  
246 failure of antiviral therapy allowed us to define the viral response to convalescent plasma,  
247 similar to a recent report on asymptomatic long term shedding with four sequences over 105  
248 days<sup>9</sup>, although the reported shifts in genetic composition of the viral population could not  
249 be explained phenotypically. Another common finding is the very low neutralisation activity  
250 in serum post transfusion of CP with waning as expected. Apart from the difference in the  
251 outcome of infection (severe, fatal disease versus asymptomatic disease and clearance),  
252 critically important differences in our study include: 1. The intensity of sampling and use of  
253 both long and short read sequencing to verify variant calls, thereby providing a unique  
254 scientific resource for longitudinal population genetic analysis. 2. The close alignment  
255 between the genetic composition of the viral population and CP administration, with an  
256 experimentally verified resistant strain emerging, falling to low frequency, and then rising  
257 again under CP selection. 3. Real time detection of emergence of a variant,  $\Delta$ H69/ $\Delta$ V70, that



258 is increasing in frequency in Europe, and shown here to affect neutralization by multiple  
259 COVID-19 patient derived sera.

260

261 We have noted in our analysis the potential influence of compartmentalised viral replication  
262 upon the sequences recovered in upper respiratory tract samples. Both population genetic  
263 and small animal studies have shown a lack of reassortment between influenza viruses within  
264 a single host during an infection, suggesting that acute respiratory viral infection may be  
265 characterised by spatially distinct viral populations<sup>17,18</sup>. In the analysis of data it is important  
266 to distinguish genetic changes which occur in the primary viral population from apparent  
267 changes that arise from the stochastic observation of spatially distinct subpopulations in the  
268 host. While the samples we observe on days 93 and 95 of infection are genetically distinct  
269 from the others, the remaining samples are consistent with arising from a consistent viral  
270 population, supporting the finding of a reversion and subsequent regain of antibody  
271 resistance. We note that in a study of SARS-CoV-2, Choi et al reported the detection in post  
272 mortem tissue of viral RNA not only in lung tissue, but also in the spleen, liver and heart<sup>7</sup>.  
273 Mixing of virus from different compartments, for example via blood, or movement of  
274 secretions from lower to upper respiratory tract, could lead to fluctuations in viral populations  
275 at particular sampling sites. Experiments in animal models with sampling of different  
276 replication sites could allow a better understanding of SARS-CoV-2 population genetics and  
277 enable prediction of escape variants following antibody based therapies.

278

279 This is a single case report and therefore limited conclusions can be drawn about  
280 generalisability.

281 In addition to documenting the emergence of SARS-CoV-2 Spike  $\Delta$ H69/ $\Delta$ V70 + D796H *in vivo*,  
282 conferring broad reduction in susceptibility to serum/plasma polyclonal, but no effect on a  
283 set of predominantly RBD-targeting monoclonal antibodies, these data highlight that  
284 infection control measures need to be specifically tailored to the needs of  
285 immunocompromised patients. The data also highlight caution in interpretation of CDC  
286 guidelines that recommend 20 days as the upper limit of infection prevention precautions in  
287 immune compromised patients who are afebrile<sup>19</sup>. Due to the difficulty with culturing clinical  
288 isolates, use of surrogates for infectious virus such as sgRNA are warranted<sup>20</sup>. However, where  
289 detection of ongoing viral evolution is possible, this serves as a clear proxy for the existence

290 of infectious virus. In our case we detected environmental contamination whilst in a single  
291 occupancy room and the patient was moved to a negative-pressure high air-change infectious  
292 disease isolation room.

293

294 The clinical efficacy of CP has been called into question recently<sup>21</sup>, and our data suggest  
295 caution in use of CP in patients with immune suppression of both T cell and B cell arms. In  
296 such cases, the antibodies administered have little support from cytotoxic T cells, thereby  
297 reducing chances of clearance and raising the potential for escape mutations. Whilst we await  
298 further data, CP administered for clinical need in immune suppression, should ideally be  
299 undertaken in single occupancy rooms with enhanced infection control precautions, including  
300 SARS-CoV-2 environmental sampling and real-time sequencing.

301

302

303

304

305

306

307

308

309

310

311

312

313

314

315

316

317

318

319

320

321 **Table 1: Neutralisation activity of convalescent plasma and patient sera taken in between**  
 322 **CP doses against SARS-CoV-2 viral variants observed in A. patient case. B. five patients with**  
 323 **recovered COVID-19.** Shown are IC50 dilution titres - the CP or serum reciprocal dilution at  
 324 which 50% of virus infectivity is lost against wild type (baseline) or D796H + Δ69/70 mutant  
 325 Spike protein expressed on the surface of a lentiviral particle. Fold change is the difference  
 326 between the two viruses, and values below 1 indicate that the D796H/Δ69/70 mutant is less  
 327 sensitive to the CP or serum. Only the D66 serum sample failed to demonstrate significantly  
 328 higher resistance of the D796H/Δ69/70 mutant.

329

A.	IC50 as reciprocal dilution (95% CI)		Fold Change IC50 (95% CI)
	WT	D796H + Δ69/70	
CP1	2480.0 (2104.0 - 2965.0)	924.2 (634.1 - 1316.0)	0.37 (0.24 - 0.56)
D64 serum	163.7 (106.6 - 256.4)	55.6 (29.5 - 100.6)	0.27 (0.12 - 0.77)
CP2	447.1 (305.2 - 670.1)	196 (129.8 - 294.7)	0.47 (0.25 - 0.86)
D66 serum	175.7 (90.7 - 410.4)	85.5 (48.2 - 149.8)	0.82 (0.29 - 1.96)
CP3	280.2 (172.8 - 480.3)	115 (75.0 - 175.5)	0.47 (0.24 - 0.91)

330

331

332

333

334

B.	IC50 as reciprocal dilution (95% CI)		Fold Change IC50 (95% CI)
	WT	D796H + Δ69/70	
Serum 1	994.1 (852.7-1159.0)	755.8 (426.7-1269.0)	0.71 (0.39-1.33)
Serum 2	2107.0 (1680.0-2662.0)	1045.0 (745.9-1387.0)	0.42 (0.27-0.70)
Serum 3	3241.0 (2377.0-4643.0)	347.4 (234.4-505.4)	0.11 (0.07-0.17)
Serum 4	17368.0 (14357.0-22130.0)	2965.0 (2287.0-3767.0)	0.26 (0.20-0.32)
Serum 5	52735.0 (34276.0-93957.0)	3871.0 (3525.0-4252.0)	0.20 (0.17-0.24)

335

336

337

338

339

340

341

342

343 **Ethics**

344 The study was approved by the East of England – Cambridge Central Research Ethics  
345 Committee (17/EE/0025). The patient and family provided written informed consent.  
346 Additional controls with COVID-19 were enrolled to the NIHR BioResource Centre Cambridge  
347 under ethics review board (17/EE/0025).

348

349 **Acknowledgements**

350 We are immensely grateful to the patient and family. We would also like to thank the staff at  
351 CUH and the NIHR Cambridge Clinical Research Facility. We would like to thank Dr Ruthiran  
352 Kugathasan and Professor Wendy Barclay for helpful discussions and Dr Martin Curran, Dr  
353 William Hamilton and Dr. Dominic Sparkes. We would like to thank Prof Andres Floto and Prof  
354 Ferdia Gallagher. We thank Dr James Voss for the kind gift of HeLa cells stably expressing  
355 ACE2. COG-UK is supported by funding from the Medical Research Council (MRC) part of UK  
356 Research & Innovation (UKRI), the National Institute of Health Research (NIHR) and Genome  
357 Research Limited, operating as the Wellcome Sanger Institute. RKG is supported by a  
358 Wellcome Trust Senior Fellowship in Clinical Science (WT108082AIA). LEM is supported by a  
359 Medical Research Council Career Development Award (MR/R008698/1). SAK is supported by  
360 the Bill and Melinda Gates Foundation via PANGEA grant: OPP1175094. DAC is supported by  
361 a Wellcome Trust Clinical PhD Research Fellowship. CJRI acknowledges MRC funding (ref:  
362 MC\_UU\_00002/11). This research was supported by the National Institute for Health  
363 Research (NIHR) Cambridge Biomedical Research Centre, the Cambridge Clinical Trials Unit  
364 (CCTU) and by the UCL Coronavirus Response Fund and made possible through generous  
365 donations from UCL's supporters, alumni and friends (LEM). JAGB is supported by the Medical  
366 Research Council (MC\_UP\_1201/16).

367

368 **Author contributions**

369 Conceived study: RKG, SAK, DAC, AS, TG, EGK

370 Designed experiments: RKG, SAK, DAC, LEM, JAGB, EGK, AC, NT, AC, CS

371 Performed experiments: SAK, DAC, LEM, RD, CRS, AJ, IATMF, KS, TG, CJRI, BB, JS, MJvG

372 Interpreted data: RKG, SAK, DAC, PM, LEM, JAGB, PM, SG, KS, TG, JB, KGCS, IG, CJRI, JAGB,  
373 IUL, DR, JS, BB

374

## 375 **Methods**

### 376 *Clinical Sample Collection and Next generation sequencing*

377 Serial samples were collected from the patient periodically from the lower respiratory tract  
378 (sputum or endotracheal aspirate), upper respiratory tract (throat and nasal swab), and from  
379 stool. Nucleic acid extraction was done from 500µl of sample with a dilution of MS2  
380 bacteriophage to act as an internal control, using the easyMAG platform (Biomerieux, Marcy  
381 L'Etoile) according to the manufacturers' instructions. All samples were tested for presence of  
382 SARS-CoV-2 with a validated one-step RT q-PCR assay developed in conjunction with the  
383 Public Health England Clinical Microbiology <sup>22</sup>. Amplification reaction were all performed on  
384 a Rotorgene™ PCR instrument. Samples which generated a CT of ≤36 were considered to be  
385 positive.

386

387 Sera from recovered patients in the COVIDx study<sup>23</sup> were used for testing of neutralisation  
388 activity by SARS-CoV-2 mutants.

389

390 For viral genomic sequencing, total RNA was extracted from samples as described. Samples  
391 were sequenced using MinION flow cells version 9.4.1 (Oxford Nanopore Technologies)  
392 following the ARTICnetwork V3 protocol  
393 (<https://dx.doi.org/10.17504/protocols.io.bbmuik6w>) and BAM files assembled using the  
394 ARTICnetwork assembly pipeline ([https://artic.network/ncov-2019/ncov2019-](https://artic.network/ncov-2019/ncov2019-bioinformatics-sop.html)  
395 [bioinformatics-sop.html](https://artic.network/ncov-2019/ncov2019-bioinformatics-sop.html)). A representative set of 10 sequences were selected and also  
396 sequenced using the Illumina MiSeq platform. Amplicons were diluted to 2 ng/µl and 25 µl  
397 (50 ng) were used as input for each library preparation reaction. The library preparation used  
398 KAPA Hyper Prep kit (Roche) according to manufacturer's instructions. Briefly, amplicons  
399 were end-repaired and had A-overhang added; these were then ligated with 15mM of NEXTflex  
400 DNA Barcodes (Bio Scientific, Texas, USA). Post-ligation products were cleaned using AMPure  
401 beads and eluted in 25 µl. Then, 20 µl were used for library amplification by 5 cycles of PCR.  
402 For the negative controls, 1ng was used for ligation-based library preparation. All libraries  
403 were assayed using TapeStation (Agilent Technologies, California, USA) to assess fragment  
404 size and quantified by QPCR. All libraries were then pooled in equimolar accordingly. Libraries  
405 were loaded at 15nM and spiked in 5% PhiX (Illumina, California, USA) and sequenced on one

406 MiSeq 500 cycle using a Miseq Nano v2 with 2x 250 paired-end sequencing. A minimum of  
407 ten reads were required for a variant call.

408

#### 409 *Bioinformatics Processes*

410 For long-read sequencing, genomes were assembled with reference-based assembly and a  
411 curated bioinformatics pipeline with 20x minimum coverage across the whole-genome<sup>24</sup>. For  
412 short-read sequencing, FASTQs were downloaded, poor-quality reads were identified and  
413 removed, and both Illumina and PHiX adapters were removed using TrimGalore v0.6.6<sup>25</sup>.  
414 Trimmed paired-end reads were mapped to the National Center for Biotechnology  
415 Information SARS-CoV-2 reference sequence MN908947.3 using MiniMap2-2.17 with  
416 arguments -ax and sr<sup>26</sup>. BAM files were then sorted and indexed with samtools v1.11 and PCR  
417 optical duplicates removed using Picard (<http://broadinstitute.github.io/picard>). Single  
418 nucleotide polymorphisms (SNPs) were called using Freebayes v1.3.2<sup>27</sup> with a ploidy setting  
419 of 1, minimum allele frequency of 0.20 and a minimum depth of five reads. Finally, a  
420 consensus sequences of nucleic acids with a minimum whole-genome coverage of at least  
421 20x were generated with BCFtools using a 0% majority threshold.

422

#### 423 *Phylogenetic Analysis*

424 All available full-genome SARS-CoV-2 sequences were downloaded from the GISAID database  
425 (<http://gisaid.org/>)<sup>28</sup> on 17<sup>th</sup> September. Duplicate and low-quality sequences (>5% N  
426 regions) were removed, leaving a dataset of 138,472 sequences with a length of >29,000bp.  
427 All sequences were sorted by name and only sequences sequenced with United Kingdom /  
428 England identifiers were retained. From this dataset, a subset of 250 sequences were  
429 randomly subsampled using seqtk (<https://github.com/lh3/seqtk>). These 250 sequences were  
430 aligned to the 23 patient sequences, as well as three other control patients (persistent long-  
431 term shedders from the same hospital) (Supplementary Table 2) and the SARS-CoV-2  
432 reference strain MN908947.3, using MAFFT v7.473 with automatic flavour selection<sup>29</sup>. Major  
433 SARS-CoV-2 clade memberships were assigned to all sequences using the Nextclade server  
434 v0.8 (<https://clades.nextstrain.org/>).

435

436 Maximum likelihood phylogenetic trees were produced using the above curated dataset using  
437 IQ-TREE v2.1.2<sup>30</sup>. Evolutionary model selection for trees were inferred using ModelFinder<sup>31</sup>

438 and trees were estimated using the GTR+F+I model with 1000 ultrafast bootstrap replicates  
439 <sup>32</sup>. All trees were visualised with Figtree v.1.4.4 (<http://tree.bio.ed.ac.uk/software/figtree/>),  
440 rooted on the SARS-CoV-2 reference sequence and nodes arranged in descending order.  
441 Nodes with bootstraps values of <50 were collapsed using an in-house script.

442

443 A time tree indicating temporal divergence was inferred using TreeTime v0.75 <sup>33</sup>. For this a  
444 further subsample of 100 sequences from the multiple sequence alignment used to make the  
445 maximum likelihood tree were selected, which represented sequences belonging to  
446 NextStrain clade 20B. This included the 23 patient genomes, all genomes from two of the  
447 three long-term shedders (one was excluded as it belonged to NextStrain clade 19A), 75  
448 subsampled Cambridge sequences, and the SARS-CoV-2 reference strain MN908947.3. All  
449 sequences were re-aligned using MAFFT v7.473 with automatic flavour selection <sup>29</sup> and used  
450 as input.

451

452 Molecular substitution (clock) rates for the index patient, as well as three long-term shedders  
453 and two recently described immunocompromised patients from literature, were estimated  
454 using BEAST v2.6.3 <sup>34</sup> using a HKY substitution model with 4 rate categories drawn from a  
455 gamma distribution, a strict clock and a coalescent exponential population tree prior. MCMC  
456 was run for 100 million iterations excluding a 15% burn-in. Tracer v1.7.1 was used to analyse  
457 the BEAST trace in order extract the clock rate and ensure convergence had occurred.

458

#### 459 *In-depth allele frequency variant calling*

460 The SAMFIRE package<sup>35</sup> was used to call allele frequency trajectories from BAM file data.  
461 Reads were included in this analysis if they had a median PHRED score of at least 30, trimming  
462 the ends of reads to achieve this if necessary. Nucleotides were then filtered to have a PHRED  
463 score of at least 30; reads with fewer than 30 such reads were discarded. Distances between  
464 sequences, accounting for low-frequency variant information, was also conducted using  
465 SAMFIRE. The sequence distance metric, described in an earlier paper <sup>11</sup>, combines allele  
466 frequencies across the whole genome. Where L is the length of the genome, we define  $q(t)$   
467 as a  $4 \times L$  element vector describing the frequencies of each of the nucleotides A, C, G, and T  
468 at each locus in the viral genome sampled at time t. For any given locus i in the genome we



469 calculate the change in allele frequencies between the times  $t_1$  and  $t_2$  via a generalisation of  
470 the Hamming distance

471

$$472 \quad d(q_i(t_1), q_i(t_2)) = \frac{1}{2} \sum_{a \in \{A, C, G, T\}} |q_i^a(t_1) - q_i^a(t_2)|$$

473

474 where the vertical lines indicate the absolute value of the difference. These statistics were  
475 then combined across the genome to generate the pairwise sequence distance metric

476

$$477 \quad D(\mathbf{q}(t_1), \mathbf{q}(t_2)) = \sum_i d(q_i(t_1), q_i(t_2))$$

478

479 The Mathematica software package was used to conduct a regression analysis of pairwise  
480 sequence distances against time, leading to an estimate of a mean rate of within-host  
481 sequence evolution. In contrast to the phylogenetic analysis, this approach assumed the  
482 samples collected on days 93 and 95 to arise via stochastic emission from a spatially separated  
483 subpopulation within the host, leading to a lower inferred rate of viral evolution for the bulk  
484 of the viral population.

485

#### 486 *Inference of selection*

487 Under the assumption of a large effective population size, a deterministic one-locus model of  
488 selection was fitted to genome sequence data describing changes in the frequency of the  
489 variant T39I. Where  $q(t)$  represents the frequency of a single variant at time  $t$ , we used a  
490 maximum likelihood method to infer the initial variant frequency at time  $t=1$ , and the  
491 selection coefficient  $s$ , for times from the initial time point to the disappearance of the variant  
492 from the population. Specifically, where  $n(t_i)$  and  $N(t_i)$  were the number of observations of  
493 the variant and the total read depth at that locus at time  $t_i$ , we fitted the model

494

$$495 \quad q(t) = \frac{q(1)e^{st}}{1 - q(1) + q(1)e^{st}}$$

496

497 so as to maximise the binomial likelihood

498

499

$$L = \sum_i \log \binom{N_i}{n_i} q(t_i)^{n_i} (1 - q(t_i))^{N - n_i}$$

500 A similar calculation was performed to estimate the mean effective selection (incorporating  
501 intrinsic selection for the variant plus linkage with other selected alleles) acting upon the  
502 variant D796H during the final period of CP therapy. In this case selection was modelled as  
503 being time-dependent, kicking in with the administration of therapy. We fitted the model:

504

505

$$q(t) = \begin{cases} q & \text{if } t < \tau \\ \frac{q e^{s(t-\tau)}}{1 - q + q e^{s(t-\tau)}} & \text{if } t \geq \tau \end{cases}$$

506

507 to the data, setting  $\tau = 95$ .

508

#### 509 *Recombination Detection*

510 All sequences were tested for potential recombination, as this would impact on evolutionary  
511 estimates. Potential recombination events were explored with nine algorithms (RDP, MaxChi,  
512 SisScan, GeneConv, Bootscan, PhylPro, Chimera, LARD and 3SEQ), implemented in RDP5 with  
513 default settings<sup>36</sup>. To corroborate any findings, ClonalFrameML v1.12<sup>37</sup> was also used to infer  
514 recombination breakpoints. Neither programs indicated evidence of recombination in our  
515 data.

516

#### 517 *Structural Viewing*

518 The Pymol Molecular Graphics System v2.4.0 ([https://github.com/schrodinger/pymol-open-](https://github.com/schrodinger/pymol-open-source/releases)  
519 [source/releases](https://github.com/schrodinger/pymol-open-source/releases)) was used to map the location of the four spike mutations of interested onto  
520 a SARS-CoV-2 spike structure visualised by Wrobel et al (PDB: 6ZGE)<sup>38</sup>.

521

#### 522 *Generation of Spike mutants*

523 Amino acid substitutions were introduced into the D614G pCDNA\_SARS-CoV-2\_Spike plasmid  
524 as previously described<sup>39</sup> using the QuikChange Lightning Site-Directed Mutagenesis kit,  
525 following the manufacturer's instructions (Agilent Technologies, Inc., Santa Clara, CA).

526

527 *Pseudotype virus preparation*

528 Viral vectors were prepared by transfection of 293T cells by using Fugene HD transfection  
529 reagent (Promega). 293T cells were transfected with a mixture of 11ul of Fugene HD, 1µg of  
530 pCDNAΔ19Spike, 1ug of p8.91 HIV-1 gag-pol expression vector<sup>40,41</sup>, and 1.5µg of pCSFLW  
531 (expressing the firefly luciferase reporter gene with the HIV-1 packaging signal). Viral  
532 supernatant was collected at 48 and 72h after transfection, filtered through 0.45um filter  
533 and stored at -80°C. The 50% tissue culture infectious dose (TCID<sub>50</sub>) of SARS-CoV-2  
534 pseudovirus was determined using Steady-Glo Luciferase assay system (Promega).

535

536 RT activity in virion containing supernatant was measured as previously described.

537

538 *Serum/plasma pseudotype neutralisation assay*

539 Spike pseudotype assays have been shown to have similar characteristics as neutralisation  
540 testing using fully infectious wild type SARS-CoV-2<sup>12</sup>. Virus neutralisation assays were  
541 performed on 293T cell transiently transfected with ACE2 and TMPRSS2 using SARS-CoV-2  
542 Spike pseudotyped virus expressing luciferase<sup>42</sup>. Pseudotyped virus was incubated with  
543 serial dilution of heat inactivated human serum samples or convalescent plasma in duplicate  
544 for 1h at 37°C. Virus and cell only controls were also included. Then, freshly trypsinized 293T  
545 ACE2/TMPRSS2 expressing cells were added to each well. Following 48h incubation in a 5%  
546 CO<sub>2</sub> environment at 37°C, the luminescence was measured using Steady-Glo Luciferase  
547 assay system (Promega).

548

549 *mAb pseudotype neutralisation assay*

550 Virus neutralisation assays were performed on HeLa cells stably expressing ACE2 and using  
551 SARS-CoV-2 Spike pseudotyped virus expressing luciferase as previously described<sup>43</sup>.  
552 Pseudotyped virus was incubated with serial dilution of purified mAbs<sup>13</sup> in duplicate for 1h at  
553 37°C. Then, freshly trypsinized HeLa ACE2- expressing cells were added to each well.  
554 Following 48h incubation in a 5% CO<sub>2</sub> environment at 37°C, the luminescence was  
555 measured using Bright-Glo Luciferase assay system (Promega) and neutralization calculated  
556 relative to virus only controls. IC<sub>50</sub> values were calculated in Graphpad Prism.

557

## 558 References

- 559 1 Zhang, T., Wu, Q. & Zhang, Z. Probable pangolin origin of SARS-CoV-2 associated with the  
560 COVID-19 outbreak. *Current Biology* (2020).
- 561 2 Xiao, K. *et al.* Isolation of SARS-CoV-2-related coronavirus from Malayan pangolins. *Nature*  
562 **583**, 286-289, doi:10.1038/s41586-020-2313-x (2020).
- 563 3 Sanjuán, R. & Domingo-Calap, P. Mechanisms of viral mutation. *Cell Mol Life Sci* **73**, 4433-  
564 4448, doi:10.1007/s00018-016-2299-6 (2016).
- 565 4 Korber, B. *et al.* Tracking Changes in SARS-CoV-2 Spike: Evidence that D614G Increases  
566 Infectivity of the COVID-19 Virus. *Cell*, doi:10.1016/j.cell.2020.06.043 (2020).
- 567 5 Yurkovetskiy, L. *et al.* Structural and Functional Analysis of the D614G SARS-CoV-2 Spike  
568 Protein Variant. *Cell* **183**, 739-751 e738, doi:10.1016/j.cell.2020.09.032 (2020).
- 569 6 Korber, B. *et al.* Tracking changes in SARS-CoV-2 Spike: evidence that D614G increases  
570 infectivity of the COVID-19 virus. *Cell* **182**, 812-827. e819 (2020).
- 571 7 Choi, B. *et al.* Persistence and Evolution of SARS-CoV-2 in an Immunocompromised Host. *N*  
572 *Engl J Med*, doi:10.1056/NEJMc2031364 (2020).
- 573 8 McCarthy, K. R. *et al.* Natural deletions in the SARS-CoV-2 spike glycoprotein drive antibody  
574 escape. *bioRxiv*, 2020.2011.2019.389916, doi:10.1101/2020.11.19.389916 (2020).
- 575 9 Avanzato, V. A. *et al.* Case Study: Prolonged infectious SARS-CoV-2 shedding from an  
576 asymptomatic immunocompromised cancer patient. *Cell* (2020).
- 577 10 Wright, S. Size of population and breeding structure in relation to evolution. *Science*, 430-431  
578 (1938).
- 579 11 Lumby, C. K., Zhao, L., Breuer, J. & Illingworth, C. J. A large effective population size for  
580 established within-host influenza virus infection. *Elife* **9**, doi:10.7554/eLife.56915 (2020).
- 581 12 Schmidt, F. *et al.* Measuring SARS-CoV-2 neutralizing antibody activity using pseudotyped and  
582 chimeric viruses. 2020.2006.2008.140871, doi:10.1101/2020.06.08.140871 %J bioRxiv (2020).
- 583 13 Brouwer, P. J. M. *et al.* Potent neutralizing antibodies from COVID-19 patients define multiple  
584 targets of vulnerability. *Science* **369**, 643-650, doi:10.1126/science.abc5902 (2020).
- 585 14 Robbiani, D. F. *et al.* Convergent antibody responses to SARS-CoV-2 in convalescent  
586 individuals. *Nature* **584**, 437-442, doi:10.1038/s41586-020-2456-9 (2020).
- 587 15 Barnes, C. O. *et al.* Structures of Human Antibodies Bound to SARS-CoV-2 Spike Reveal  
588 Common Epitopes and Recurrent Features of Antibodies. *Cell* **182**, 828-842 e816,  
589 doi:10.1016/j.cell.2020.06.025 (2020).
- 590 16 Shrock, E. *et al.* Viral epitope profiling of COVID-19 patients reveals cross-reactivity and  
591 correlates of severity. *Science*, doi:10.1126/science.abd4250 (2020).
- 592 17 Sobel Leonard, A. *et al.* The effective rate of influenza reassortment is limited during human  
593 infection. *PLoS pathogens* **13**, e1006203, doi:10.1371/journal.ppat.1006203 (2017).
- 594 18 Richard, M., Herfst, S., Tao, H., Jacobs, N. T. & Lowen, A. C. Influenza A Virus Reassortment Is  
595 Limited by Anatomical Compartmentalization following Coinfection via Distinct Routes.  
596 *Journal of virology* **92**, doi:10.1128/JVI.02063-17 (2018).
- 597 19 CDC. *Discontinuation of Transmission-Based Precautions and Disposition of Patients with*  
598 *COVID-19 in Healthcare Settings (Interim Guidance)*,  
599 <https://www.cdc.gov/coronavirus/2019-ncov/hcp/disposition-hospitalized-patients.html>  
600 (2020).
- 601 20 Boshier, F. A. T. *et al.* Remdesivir induced viral RNA and subgenomic RNA suppression, and  
602 evolution of viral variants in SARS-CoV-2 infected patients. *medRxiv*,  
603 2020.2011.2018.20230599, doi:10.1101/2020.11.18.20230599 (2020).
- 604 21 Simonovich, V. A. *et al.* A Randomized Trial of Convalescent Plasma in Covid-19 Severe  
605 Pneumonia. *N Engl J Med*, doi:10.1056/NEJMoa2031304 (2020).
- 606 22 Meredith, L. W. *et al.* Rapid implementation of SARS-CoV-2 sequencing to investigate cases of  
607 health-care associated COVID-19: a prospective genomic surveillance study. *The Lancet*  
608 *Infectious Diseases* **20**, 1263-1272, doi:10.1016/S1473-3099(20)30562-4 (2020).

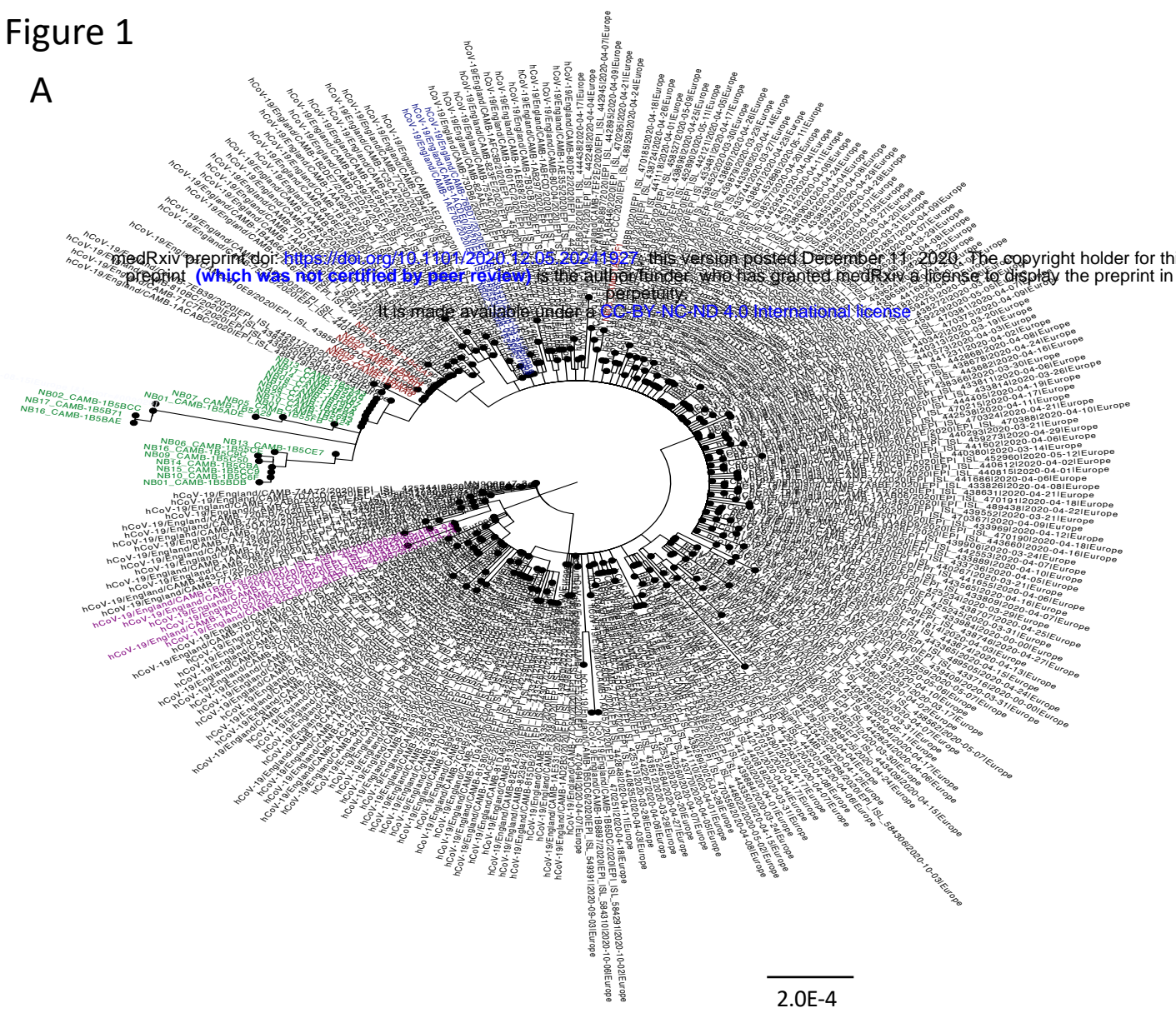
- 609 23 Collier, D. A. *et al.* Point of Care Nucleic Acid Testing for SARS-CoV-2 in Hospitalized Patients:  
610 A Clinical Validation Trial and Implementation Study. *Cell Rep Med*, 100062,  
611 doi:10.1016/j.xcrm.2020.100062 (2020).
- 612 24 Loman, N., Rowe, W. & Rambaut, A. (v1, 2020).
- 613 25 Martin, M. Cutadapt removes adapter sequences from high-throughput sequencing reads.  
614 *EMBnet. journal* **17**, 10-12 (2011).
- 615 26 Li, H. Minimap2: pairwise alignment for nucleotide sequences. *Bioinformatics (Oxford,*  
616 *England)* **34**, 3094-3100, doi:10.1093/bioinformatics/bty191 (2018).
- 617 27 Garrison, E. & Marth, G. Haplotype-based variant detection from short-read sequencing. *arXiv*  
618 *preprint arXiv:1207.3907* (2012).
- 619 28 Shu, Y. & McCauley, J. GISAID: Global initiative on sharing all influenza data - from vision to  
620 reality. *Euro surveillance : bulletin Europeen sur les maladies transmissibles = European*  
621 *communicable disease bulletin* **22**, 30494, doi:10.2807/1560-7917.ES.2017.22.13.30494  
622 (2017).
- 623 29 Katoh, K. & Standley, D. M. MAFFT Multiple Sequence Alignment Software Version 7:  
624 Improvements in Performance and Usability. *Molecular Biology and Evolution* **30**, 772-780,  
625 doi:10.1093/molbev/mst010 (2013).
- 626 30 Minh, B. Q. *et al.* IQ-TREE 2: New Models and Efficient Methods for Phylogenetic Inference in  
627 the Genomic Era. *Molecular Biology and Evolution* **37**, 1530-1534,  
628 doi:10.1093/molbev/msaa015 (2020).
- 629 31 Kalyaanamoorthy, S., Minh, B. Q., Wong, T. K. F., von Haeseler, A. & Jermini, L. S. ModelFinder:  
630 fast model selection for accurate phylogenetic estimates. *Nature Methods* **14**, 587-589,  
631 doi:10.1038/nmeth.4285 (2017).
- 632 32 Minh, B. Q., Nguyen, M. A. T. & von Haeseler, A. Ultrafast Approximation for Phylogenetic  
633 Bootstrap. *Molecular Biology and Evolution* **30**, 1188-1195, doi:10.1093/molbev/mst024  
634 (2013).
- 635 33 Sagulenko, P., Puller, V. & Neher, R. A. TreeTime: Maximum-likelihood phylodynamic analysis.  
636 *Virus evolution* **4**, vex042-vex042, doi:10.1093/ve/vex042 (2018).
- 637 34 Bouckaert, R. *et al.* BEAST 2: a software platform for Bayesian evolutionary analysis. *PLoS*  
638 *Comput Biol* **10**, e1003537 (2014).
- 639 35 Illingworth, C. J. SAMFIRE: multi-locus variant calling for time-resolved sequence data.  
640 *Bioinformatics* **32**, 2208-2209, doi:10.1093/bioinformatics/btw205 (2016).
- 641 36 Martin, D. P., Murrell, B., Golden, M., Khoosal, A. & Muhire, B. RDP4: Detection and analysis  
642 of recombination patterns in virus genomes. *Virus evolution* **1** (2015).
- 643 37 Didelot, X. & Wilson, D. J. ClonalFrameML: efficient inference of recombination in whole  
644 bacterial genomes. *PLoS Comput Biol* **11**, e1004041 (2015).
- 645 38 Wrobel, A. G. *et al.* SARS-CoV-2 and bat RaTG13 spike glycoprotein structures inform on virus  
646 evolution and furin-cleavage effects. *Nature Structural & Molecular Biology* **27**, 763-767,  
647 doi:10.1038/s41594-020-0468-7 (2020).
- 648 39 Gregson, J. *et al.* HIV-1 viral load is elevated in individuals with reverse transcriptase mutation  
649 M184V/I during virological failure of first line antiretroviral therapy and is associated with  
650 compensatory mutation L74I. *The Journal of infectious diseases*, doi:10.1093/infdis/jiz631  
651 (2019).
- 652 40 Naldini, L., Blomer, U., Gage, F. H., Trono, D. & Verma, I. M. Efficient transfer, integration, and  
653 sustained long-term expression of the transgene in adult rat brains injected with a lentiviral  
654 vector. *Proceedings of the National Academy of Sciences of the United States of America* **93**,  
655 11382-11388 (1996).
- 656 41 Gupta, R. K. *et al.* Full-length HIV-1 Gag determines protease inhibitor susceptibility within in  
657 vitro assays. *Aids* **24**, 1651-1655, doi:10.1097/QAD.0b013e3283398216 (2010).

- 658 42 Mlcochova, P. *et al.* Combined point of care nucleic acid and antibody testing for SARS-CoV-2  
659 following emergence of D614G Spike Variant. *Cell Rep Med*, 100099,  
660 doi:10.1016/j.xcrm.2020.100099 (2020).
- 661 43 Seow, J. *et al.* Longitudinal observation and decline of neutralizing antibody responses in the  
662 three months following SARS-CoV-2 infection in humans. *Nat Microbiol* **5**, 1598-1607,  
663 doi:10.1038/s41564-020-00813-8 (2020).
- 664



# Figure 1

A



B

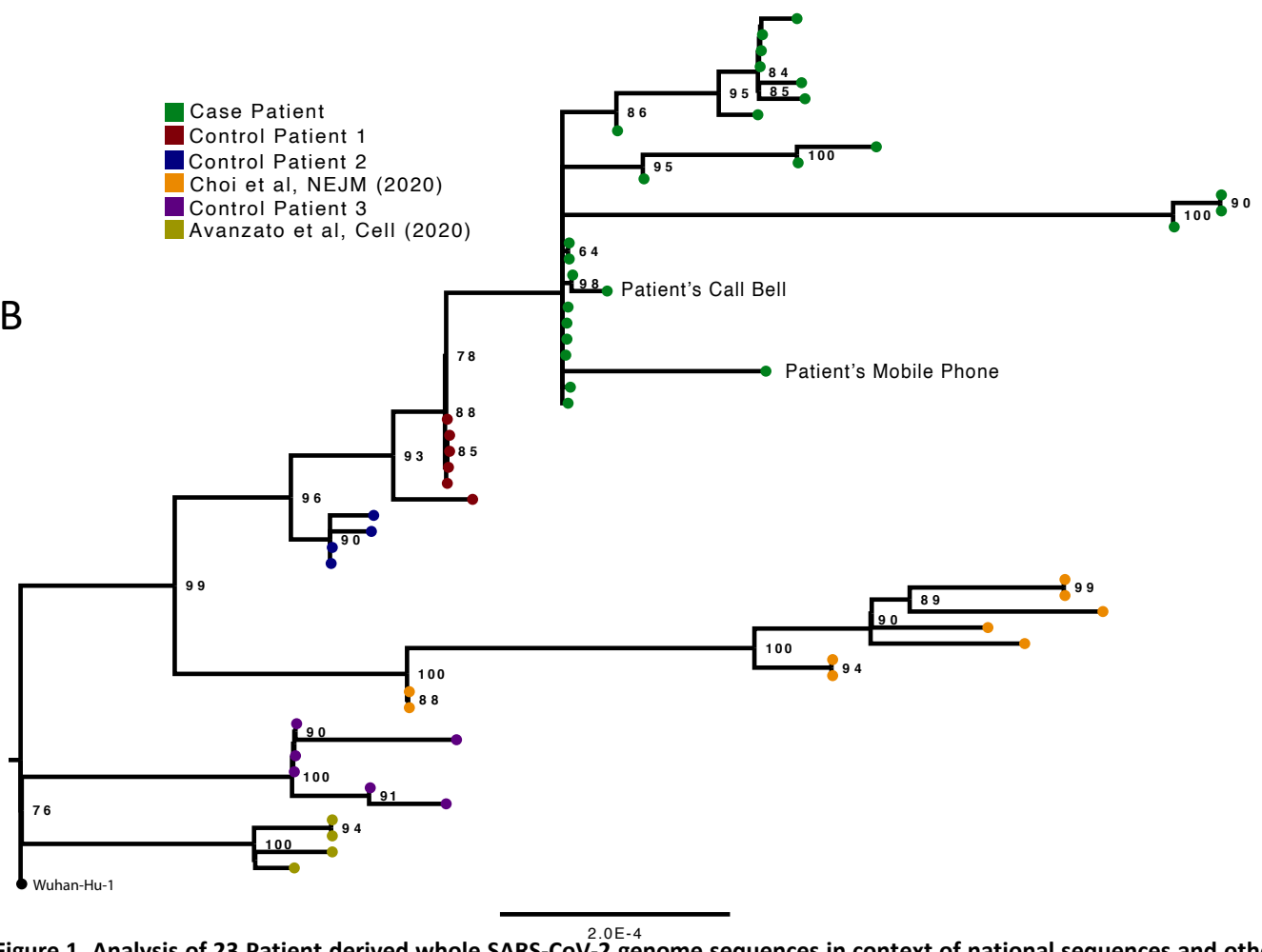
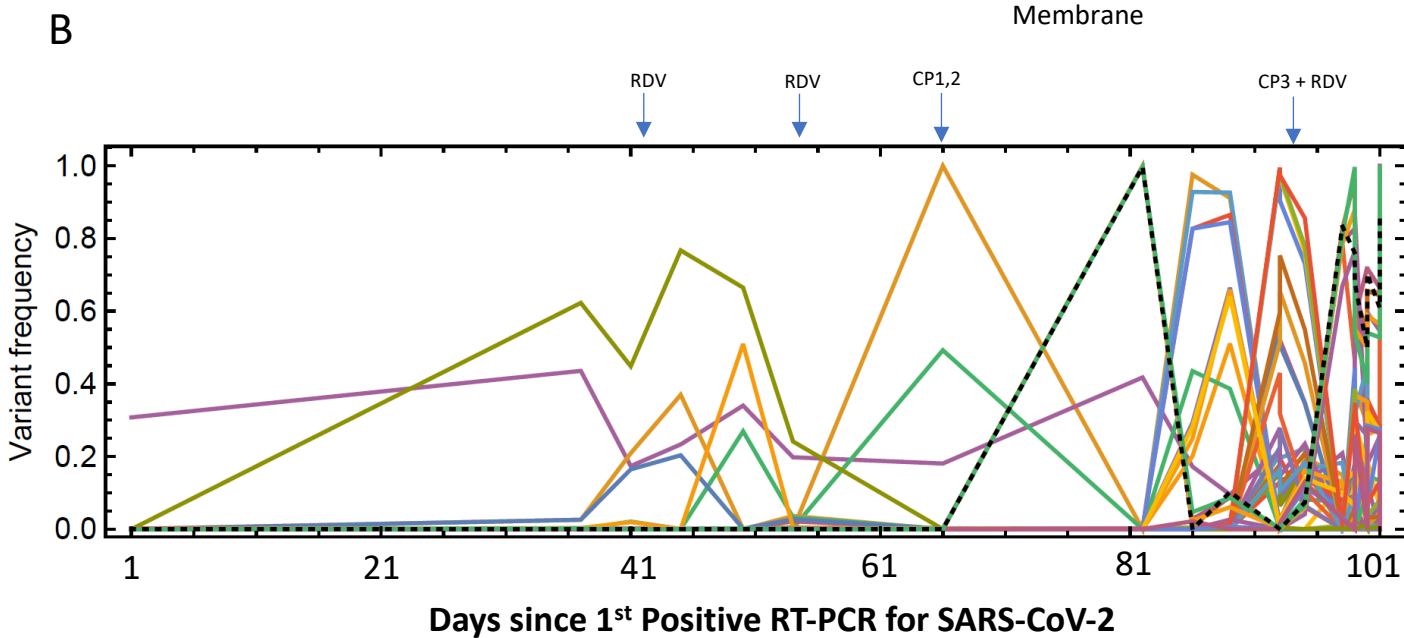
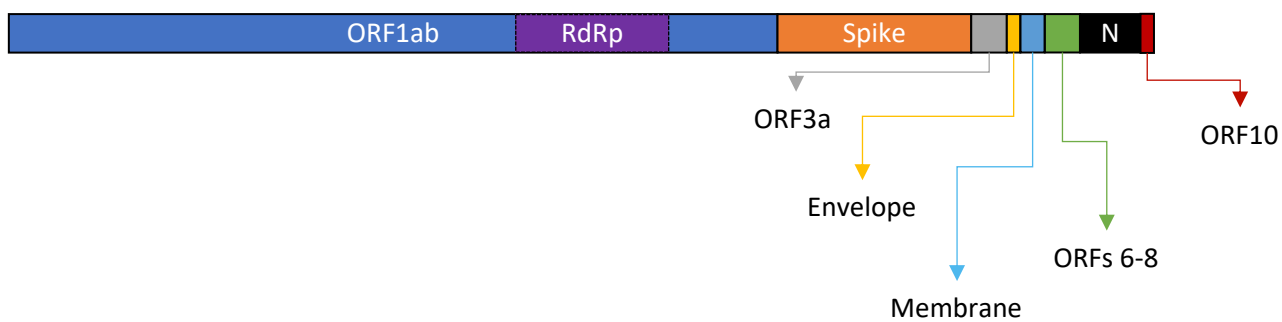
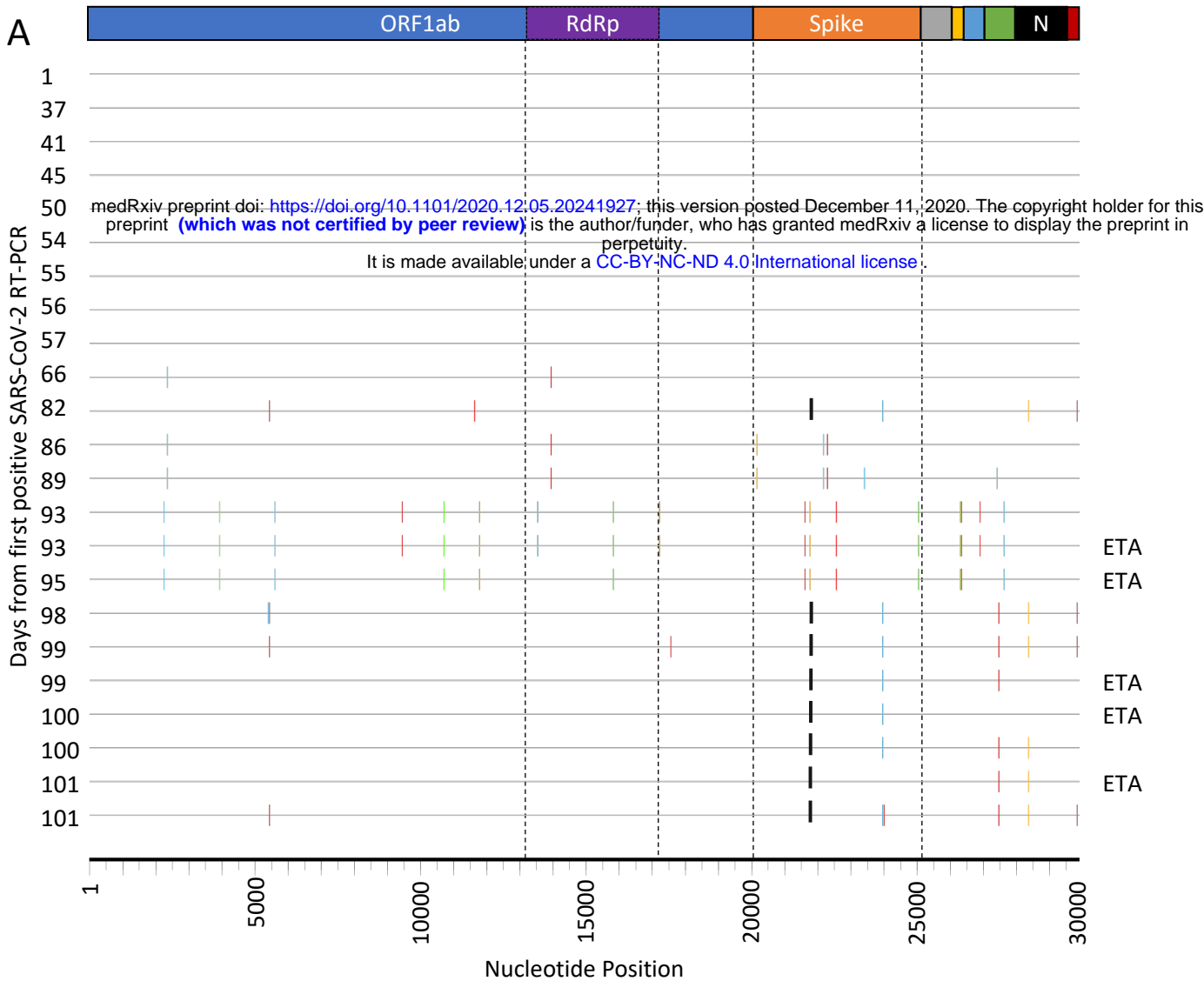


**Figure 1. Analysis of 23 Patient derived whole SARS-CoV-2 genome sequences in context of national sequences and other cases of chronic SARS-CoV-2 shedding.** A. Circularised maximum-likelihood phylogenetic tree rooted on the Wuhan-Hu-1 reference sequence, showing a subset of 250 local SARS-CoV-2 genomes from GISAID. This diagram highlights significant diversity of the case patient (green) compared to three other local patients with prolonged shedding (blue, red and purple sequences). All SARS-CoV-2 genomes were downloaded from the GISAID database and a random subset of 250 local sequences selected. B. Close-view maximum-likelihood phylogenetic tree indicating the diversity of the case patient and three other long-term shedders from the local area (red, blue and purple), compared to recently published sequences from Choi et al (orange) and Avanzato et al (gold). Control patients generally showed limited diversity temporally, though the Choi et al sequences were found to be even more divergent than the case patient. Environmental samples are indicated. 1000 ultrafast bootstraps were performed and support at nodes is indicated.



A C T G del

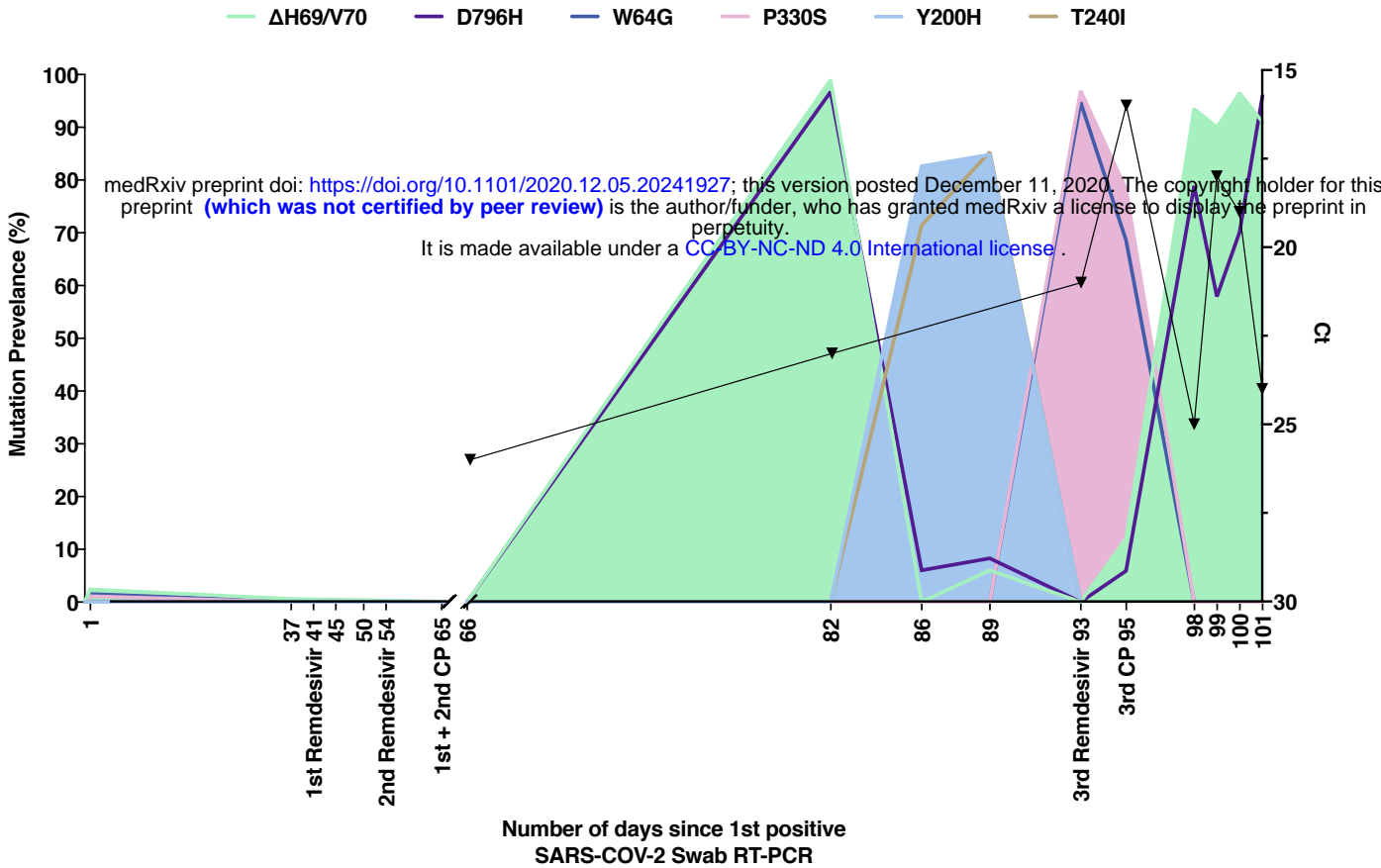
## Figure 2



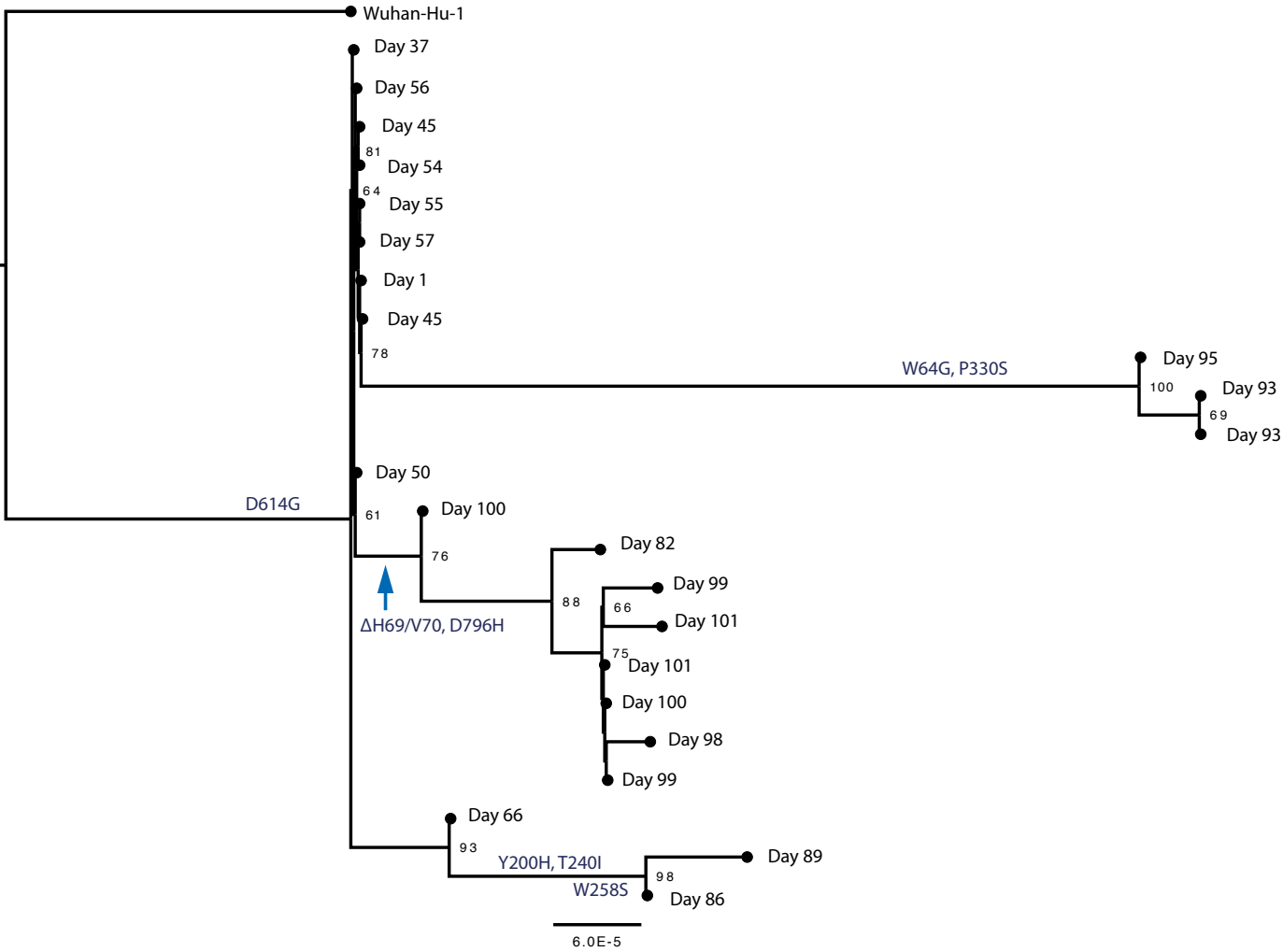
**Figure 2. Virus genetics and population structure in chronic SARS-CoV-2 infection.** **A.** Highlighter plot indicating nucleotide changes at consensus level in sequential respiratory samples compared to the consensus sequence at first diagnosis of COVID-19. Each row indicates the timepoint the sample was collected (number of days from first positive SARS-CoV-2 RT-PCR). Black dashed lines indicate the RNA-dependent RNA polymerase (RdRp) and Spike regions of the genome. Of particular interest, at consensus level, there were no nucleotide substitutions on days 1-57, despite the patient receiving two courses of remdesivir. The first major changes in the spike genome occurred on day 82, following convalescent plasma given on days 63 and 65. The double amino acid deletion in S1,  $\Delta$ H69/V70 is indicated by black lines. All samples are nose and throat swabs unless indicated with ETA (endotracheal aspirate). **B.** Whole genome amino acid variant trajectories based on Illumina short read ultra deep sequencing at 1000x coverage. All variants which reached a frequency of at least 10% in at least two samples were plotted. Black dashed line represents  $\Delta$ 69/70. CP, convalescent plasma; RDV, Remdesivir.

Figure 3

A



B



**Figure 3. Longitudinal variant frequencies and phylogenetic relationships for virus populations bearing six Spike (S) mutations** **A.** At baseline, all four S variants (Illumina sequencing) were absent (<1% and <20 reads). Approximately two weeks after receiving two units of convalescent plasma (CP), viral populations carrying  $\Delta$ H69/V70 and D796H mutants rose to frequencies >90% but decreased significantly four days later. This population was replaced by a population bearing Y200H and T240I, detected in two samples over a period of six days. These viral populations were then replaced by virus carrying W64G and P330S mutations in Spike, which both reached near fixation at day 93. Following a 3<sup>rd</sup> course of remdesivir and an additional unit of convalescent plasma, the  $\Delta$ H69/V70 and D796H virus population re-emerged to become the dominant viral strain reaching variant frequencies of >90%. Pairs of mutations arose and disappeared simultaneously indicating linkage on the same viral haplotype. **B.** Maximum likelihood phylogenetic tree of the case patient with day of sampling indicated. Spike mutations defining each of the clades are shown ancestrally on the branches on which they arose. Number at node denotes support by ultrafast bootstrapping consisting of 1000 replicates.

# Figure 4

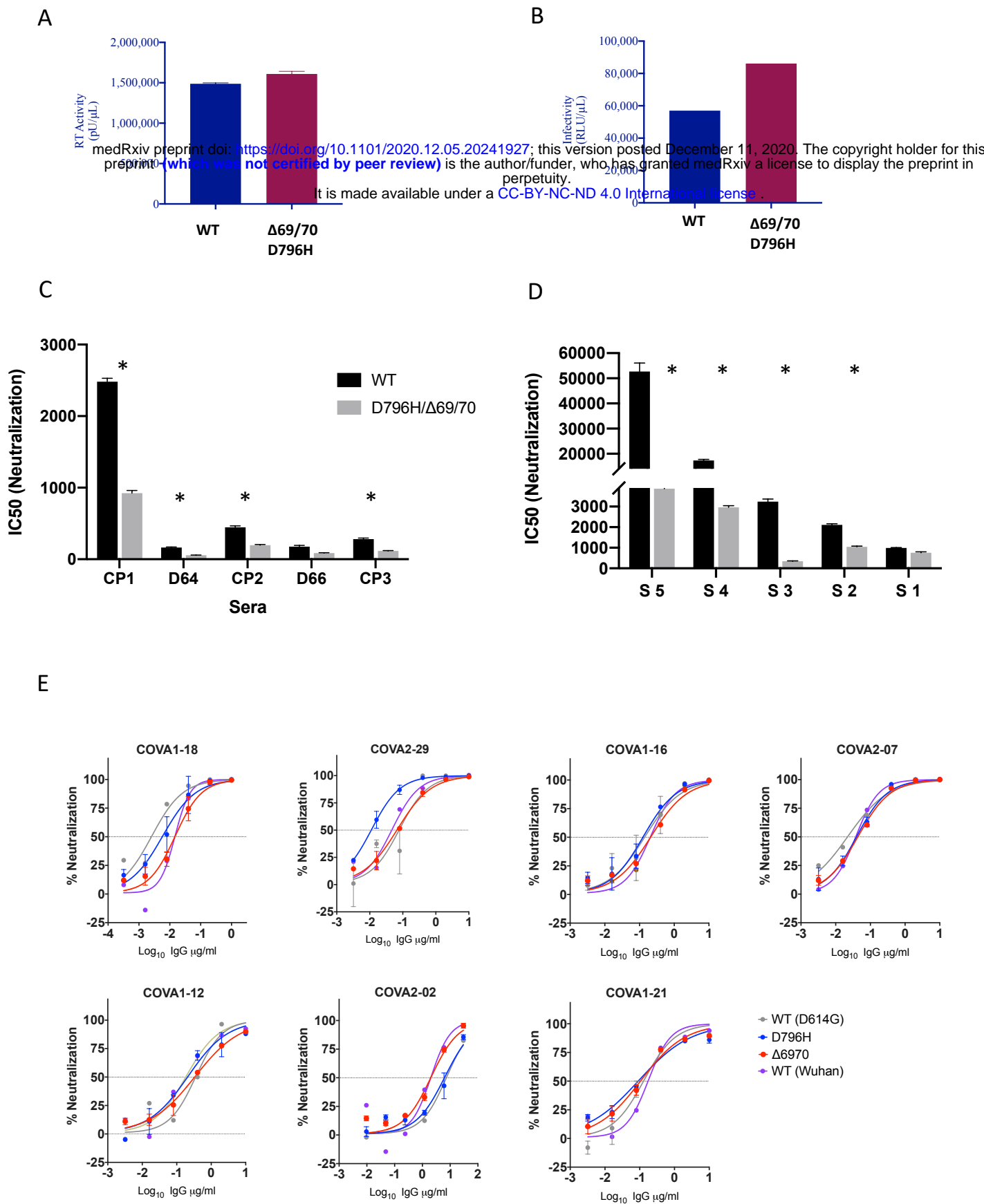


**Figure 4: Spike mutant D796H +  $\Delta$ H69/V70 has infectivity comparable to wild type but is less sensitive to multiple units of convalescent plasma (CP) and sera from recovered individuals.** **A.** Reverse transcriptase activity of virus supernatants containing lentivirus pseudotyped with SARS-CoV-2 Spike protein (WT versus mutant) **B.** Single round Infectivity of luciferase expressing lentivirus pseudotyped with SARS-CoV-2 Spike protein (WT versus mutant) on 293T cells co-transfected with ACE2 and TMPRSS2 plasmids. **C.** Patient serum (taken at indicated Day (D) ) and convalescent plasma (CP units 1-3) neutralization potency against Spike mutant D796H +  $\Delta$ H69/V70 measured using lentivirus pseudotyped with SARS-CoV-2 Spike protein (WT versus mutant). Indicated is serum dilution required to inhibit 50% of virus infection. **D.** Neutralization potency of sera from 5 unselected convalescent patients (with previous confirmed SARS-CoV-2 infection) against WT versus mutant virus as in panel C. **E** Neutralization potency of a panel of monoclonal antibodies against lentivirus pseudotyped with SARS-CoV-2 Spike protein (WT Wuhan versus single mutants D614G, D796H,  $\Delta$ H69/V70). Data are representative of at least two independent experiments \*  $p < 0.05$

Figure 5

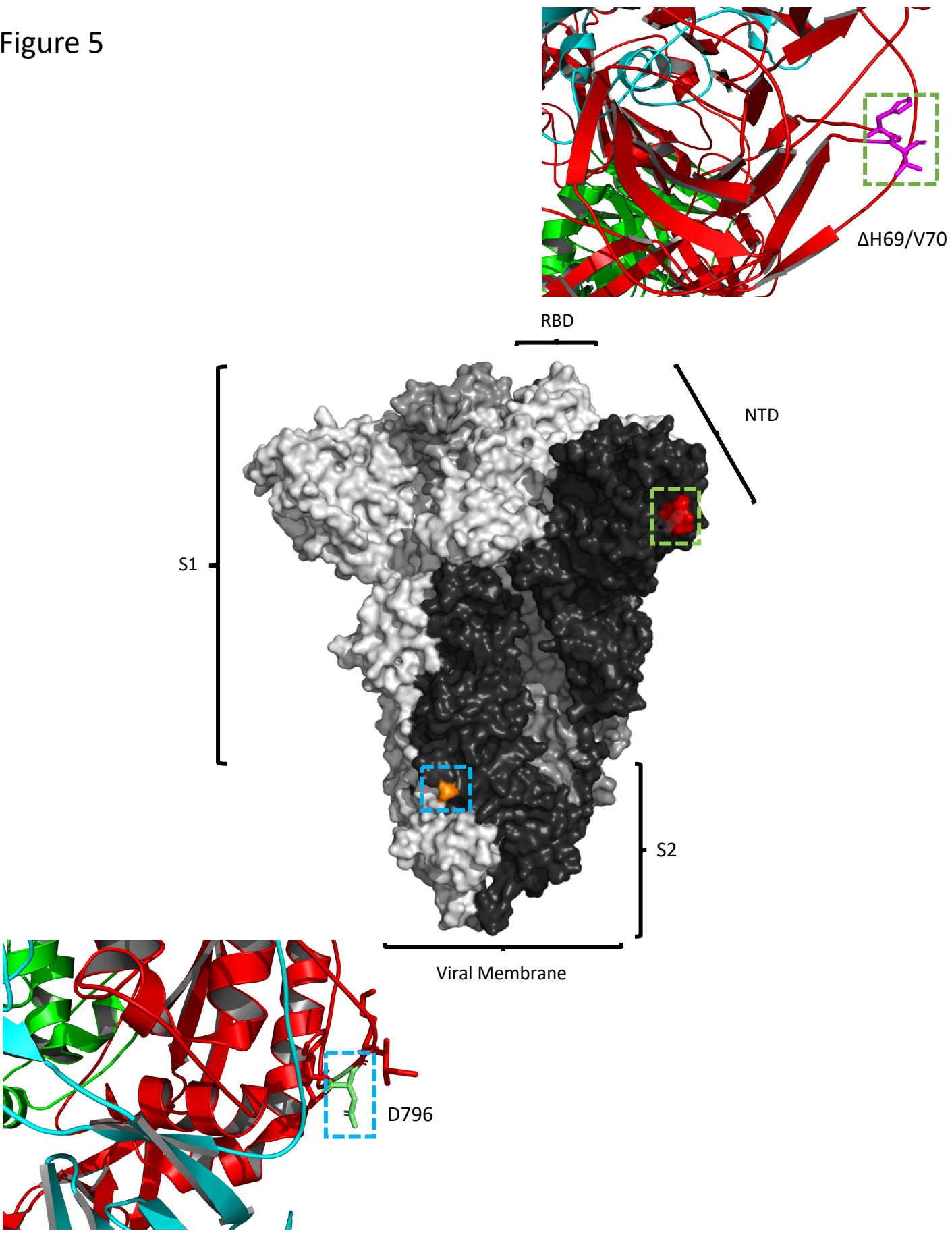


**Figure 5. Location of Spike mutations  $\Delta$ H69/Y70 in S1 and D796H in S2.** Amino acid residues H69 and Y70 deleted in the N-terminal domain (red) and D796H in subunit 2 (orange) are highlighted on a SARS-CoV-2 spike trimer (PDB: 6ZGE Wrobel et al., 2020). Each of the three protomers making up the Spike homotrimer are coloured separately in shades of grey (centre). Close-ups of  $\Delta$ H69/Y70 (above) and D796H (below) are shown in cartoon, stick representation. Both mutations are in exposed loops.